

# Predicting the mechanical properties of spring networks

Doron Grossman<sup>1,\*</sup> and Jean-Francois Joanny<sup>1</sup>

<sup>1</sup>College de France, 11 Pl. Marcelin Berthelot, 75231 Paris

(Dated: December 18, 2023)

The mechanical properties of tissues play an essential role for all tissue properties such as cell division, and differentiation or morphogenesis. Here, we study theoretically the rheology of 2-dimensional epithelial tissues described by a discrete vertex-like model, using an analytical coarse-grained continuum formulation. We show that epithelial tissues are most often shear-thinning under constant shear rate, and in certain circumstances cross over from shear thickening at low shear rates to shear thinning at high shear rates. We give an analytical expression of the tissue response in an oscillating strain experiment in the linear regime, and calculate it numerically in the non-linear regime. When the tissue is supported by an oscillating substrate, it reorients depending on frequency and substrate's Poisson's ratio. Reorientation could be gradual or abrupt, depending on tissue and substrate parameters, and the configuration phase space exhibits a tricritical point.

A biological living tissue subject to external stresses or strains, behaves as an active viscoelastic or visco-plastic material, within which various cellular processes allow for the creation and dissipation of internal stresses. The exact nature of the relevant dissipative processes depends on the type of tissue as well as on the interaction with its environment. Plant tissues behave as viscoelastic solids, in which turgor pressure and osmotic balance within the tissue play a significant role in setting both the shape and the mechanical response to deformations [1, 2]. Animal tissues, on the other hand, behave as viscoelastic or viscoplastic fluids, for which stress relaxation is driven by cell proliferation (division and apoptosis) and relative cellular rearrangements [3].

Vertex models are discrete models often used to describe all types of cellular media, in which cells are described as confluent polygons in two dimensions or polyhedra in 3 dimensions. [4–10]. They have been used very successfully to describe the behavior of squamous epithelia [11, 12]. In this paper we study the rheological properties of tissues described by the generalized 2-dimensional vertex model that we introduced in Ref. [13]. In the standard vertex model, each cell has a preferred area  $A_i^0$  and a preferred perimeter  $P_i^0$ . In the generalized model we replace the perimeter  $P = \sum_e \ell_e$  (sum of the lengths of the edges of a cell) by the generalized perimeter,  ${}^2P = \sum_e \ell_e^2$  (sum of the squared lengths of the edges of each cell), in order to allow for simpler analytical calculations, in a rigorous and justified manner. Each cell has then a preferred generalized perimeter  ${}^2P_i^0$ . The energy of the generalized vertex model has the same form as that of the original formulation

$$E = \sum_i \hat{k}_A \left( A_i - \hat{A}_i^0 \right)^2 + k_p \left( {}^2P_i - {}^2P_i^0 \right)^2. \quad (1)$$

where  $\hat{k}_A$  and  $k_p$  are positive area and perimeter moduli and  $A_i$  and  ${}^2P_i$  the actual area and perimeter of a given cell indexed by  $i$ . We checked explicitly in Ref. [13] that

the generalized vertex model leads quantitatively to the same behavior as the standard vertex model at linear order in the differences of area and perimeter with the reference area and perimeter and to a similar qualitative behavior beyond linear order, using examples where the tissue behavior is known.

In Ref. [13] we also developed a coarse-grained continuum formulation of our generalized vertex model in a hydrodynamic limit where the locally averaged cell area and perimeter vary over distances that are much larger than the cell size. In the mean field approximation where we ignore terms containing gradients of the average area and perimeter, we obtain the continuum energy as a function of two tensors defined locally. The metric tensor  $\mathbf{g}$  (with components  $g_{\mu\nu}$ , and determinant  $g$ ) prescribes the distance within the tissue using a reference state that evolves with time because of the topological transitions in the tissue. The network tensor,  $\mathbf{Q}$  (with components  $Q^{\mu\nu}$ , and determinant  $Q$ ) is defined in the reference state and prescribes the local cellular shape. Formally,  $Q^{\mu\nu}$  is given by -

$$Q^{\mu\nu} = \langle \sum_e \Delta x_e^\mu \Delta x_e^\nu \rangle = \frac{1}{N_{cells}} \sum_i \sum_{e \in i} \Delta x_e^\mu \Delta x_e^\nu \quad (2)$$

where the triangular parentheses indicate a local average defined on the right hand side where  $N_{cells}$  is the number of cells in the region under averaging,  $i$  is a cell index  $e \in i$  is an edge index of the  $i^{th}$  cell,  $\Delta x_e^\mu$  is the  $\mu$  coordinate of the vector joining the two vertices of the edge  $e$ . The energy of the tissue is then

$$E = \int \rho(x) \left\{ k_A \left( \sqrt{gQ} - A^0(x) \right)^2 + k_p \left( g_{\mu\nu} Q^{\mu\nu} - {}^2P^0(x) \right)^2 \right\} \sqrt{g} dx. \quad (3)$$

After rescaling numerical prefactors, the area of a cell is approximated by  $A = \sqrt{gQ}$  and the perimeter of a cell is the trace  ${}^2P = g_{\mu\nu} Q^{\mu\nu}$ . The rescaling changes the area

modulus to a value  $k_A$ . Changes in the metric describe how the tissue as a whole deforms and occupies space (elastic deformation), while changes in the network tensor indicate how the tissue's internal structure changes, i.e how the cells rearrange (plastic deformation).

One of the important predictions of the standard vertex model [7, 14] is the existence of a solid-solid transition between a hard isotropic solid tissue and a soft oriented solid tissue at a critical shape parameter  $p = \frac{P^0}{\sqrt{A^0}} = 3.722$ . Due to our reformulation, this transition occurs at a shape parameter  $p = \sqrt{2}P^0/A_0 = 2$ , if fluctuations of area and perimeter are ignored. When the shape parameter is larger than 2, cells have an elongated shape and the tissue is completely relaxed without any residual internal stresses. When the shape parameter is smaller than 2, cells are isotropic but the tissue has residual internal stresses. The existence of residual stresses plays an essential role for the mechanical properties of the tissue. In the following, we fix the length scale and the energy scale by imposing  $A_0 = 1$  and  $k_A = 1$ .

In this paper, we study the linear and the non-linear rheology of a 2 dimensional tissue described by the generalized vertex model in two different geometries. We first study a free standing tissue with an imposed shear rate both when the shear rate is constant and when it oscillates at a finite pulsation  $\omega$ . In a second part, we study a tissue supported by an elastic substrate, with a Poisson ratio  $\nu$ , stretched and relaxed in one direction in an oscillatory manner [15, 16].

All of the results presented here are new in the context of vertex models, and could not be calculated analytically without the continuum model we developed in [13]. The continuum model used here is valid as long as cell size is smaller than the scale over which the metric changes.

## SHEARED TISSUE

In a constant shear experiment, the tissue is directly sheared along one edge, and the steady state stresses are measured as a function of the applied shear rate  $\dot{\gamma}$ . The geometry is chosen so that the velocity is in the  $x$ , shearing the originally perpendicular  $y$  direction (see inset in Fig. 1). The shear rate defines the metric tensor

$$g_{\mu\nu} = \begin{pmatrix} 1 & \dot{\gamma}t \\ \dot{\gamma}t & 1 + \dot{\gamma}^2 t^2 \end{pmatrix}, \quad (4)$$

Given this metric tensor, we study the relaxation of the network tensor driven by the relaxation dynamics introduced in Ref. [13].

$$\partial_t Q^{\mu\nu} = -\Gamma^{\mu\nu\alpha\beta} \frac{\delta E}{\delta Q^{\alpha\beta}} - \xi_0 Q^{\mu\nu} \quad (5)$$

where  $\eta_{\alpha\beta} = \frac{\delta E}{\delta Q^{\alpha\beta}}$  is the conjugate field to the network tensor  $Q^{\alpha\beta}$ , and  $\Gamma^{\mu\nu\alpha\beta} = H_1 \left[ \frac{1}{2} (Q^{\alpha\mu} Q^{\beta\nu} + Q^{\alpha\nu} Q^{\beta\mu}) + H Q^{\alpha\beta} Q^{\mu\nu} \right]$  is the relaxation rate tensor. The rate  $H_1$  associated to the topological transitions in the tissue fixes the time scale and we choose in the following the time unit so that  $H_1 = 1$ . The dimensionless coefficient  $H$  measures the relative importance of the various topological transitions (proliferation versus  $T_1$  transitions). For pure  $T_1$  transitions that conserve the cell area (no proliferation),  $H = -\frac{1}{2}$ . The last term is due to the active proliferation of the cells (cell division and cell death), with a proliferation rate  $\xi_0$ . Note that the actual proliferation rate depends on the stresses in the system and is therefore different from the bare active proliferation rate  $\xi_0$ .

Rheological experiments measure stresses. In our model the Cauchy stress is given by

$$\sigma^{\mu\nu} = \left( \sqrt{gQ} - 1 \right) g^{\mu\nu} + 2 \frac{k_p}{\sqrt{gQ}} (g_{\alpha\beta} Q^{\alpha\beta} - p) Q^{\mu\nu}. \quad (6)$$

As the metric tensor is time dependent, it is convenient to define the time dependent flat-frame, in which the metric tensor is the unit tensor. In this frame, the network tensor describes the observable network structure in real space. The coordinate transformation uses the elongation tensor  $F_\alpha^\mu(t)$ , which transforms the coordinates in the reference frame into the actual coordinates in real space. It is such that  $(F^{-1})_\alpha^\mu (F^{-1})_\beta^\nu g_{\mu\nu} = \delta_{\alpha\beta}$ . In this frame, the network tensor reads

$$Q^{*\mu\nu} = F_\alpha^\mu F_\beta^\nu Q^{\alpha\beta}. \quad (7)$$

The time derivative of the observable network tensor  $\partial_t Q^{*\mu\nu}$ , is obtained from eq. (5)

$$\begin{aligned} \partial_t Q^* &= -\frac{Q^*}{2\sqrt{Q^*}} \left[ (1 + 2H) [(Q^* - 1) - k_p (\text{Tr} Q^* - p)]^2 \right. \\ &\quad \left. + 4k_p (\text{Tr} Q^* - p) (Q^* + H \text{Tr} Q^*) \right] - \xi_0 Q^* + \lambda, \quad (8) \end{aligned}$$

The last term is the driving force of the deformation due to the imposed shear:  $\lambda^{\mu\nu} = \partial_t F_\alpha^\mu (F^{-1})_\gamma^\alpha Q^{*\gamma\nu} + Q^{*\mu\gamma} (F^{-1})_\gamma^\alpha \partial_t F_\alpha^\nu$ . It is given explicitly by

$$\lambda = \begin{pmatrix} 0 & \dot{\gamma} Q^{*xx} \\ \dot{\gamma} Q^{*xx} & 2\dot{\gamma} Q^{*xy} \end{pmatrix} \quad (9)$$

The determinant of the observable network tensor gives the area of the cells. It is obtained from the following dynamical equation, which is independent of the forcing term  $\lambda$

$$\partial_t Q^* = -Q^{*1/2} (1 + 2H) (Q^* - 1 + k_p (\text{Tr}^2 Q^* - p^2)) - 2Q^* \xi_0 \quad (10)$$

We first study the case where there is no active cell division ( $\xi_0 = 0$ ) and the number of cells is constant. This corresponds to  $H = -1/2$  and cells can only move

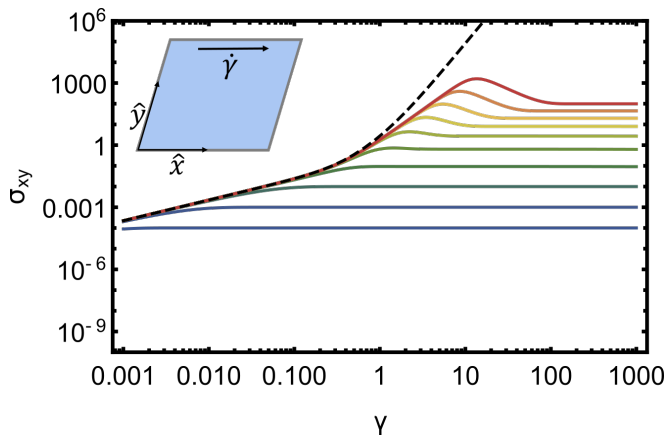


FIG. 1: Shear stress as a function of strain, at constant shear rate, when  $p = 1.5 < 2$  and  $H = -1/2$ . The colored lines correspond to different shear rates: blue (bottom plot) -  $\dot{\gamma} = 10^{-4}$ , red (top plot) -  $\dot{\gamma} = 10^5$ . The dashed black line represents the pure elastic response of a tissue with no relaxation due to topological transitions. Inset- visualization the simple shear mode with a given shear rate  $\dot{\gamma}$

past each other and exchange neighbors by  $T_1$  topological transitions. The determinant of the observable network tensor and the cell area are then constant as imposed by (10): for a soft solid tissue, when  $p > 2$  the cell area  $A_s$  is given by  $A_s = Q^{*1/2} = 1$ , whereas for a hard solid tissue, when  $p < 2$ ,  $A_s = \frac{1+2k_p p}{1+4k_p}$ .

We solved numerically the dynamical equation for the network tensor (8) and calculated the shear stress as a function of time for a given shear rate. The result is plotted as a function of the strain  $\gamma = \dot{\gamma}t$ , in figure 1 for a hard solid tissue ( $p < 2$ ) and in figure 2 for a soft solid tissue ( $p > 2$ ). In both cases the tissue is a thixotropic fluid with a time dependent shear thinning behavior. For a hard solid tissue, at small strains ( $\gamma \ll 1$ ) corresponding to short times after applications of the shear rate, the tissue behaves as an elastic solid and shear stress is proportional to strain. The elastic shear modulus can be calculated directly from the vertex model in the absence of topological transformations, by expanding the energy to second order in strain,

$$G = 2 \frac{2-p}{1+4k_p} \quad (11)$$

At larger strains, the stress overshoots and then decays to a constant value at long times that only depends on shear rate. At low rates, the stress is proportional to the shear rate defining the tissue shear viscosity discussed below. At higher shear rate, the tissue is shear thinning. A similar behavior is observed for a soft solid but the shear modulus vanishes and at short times the

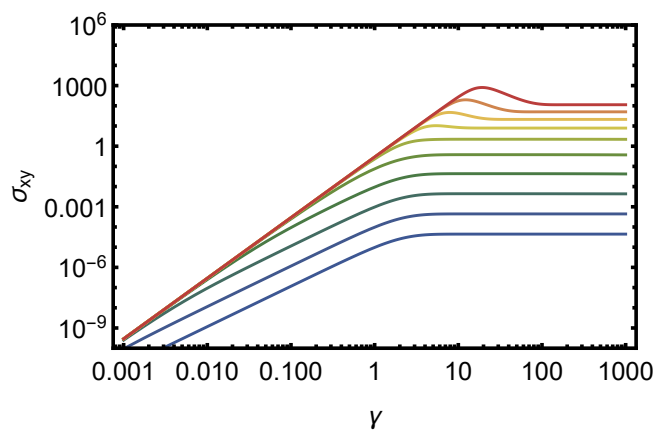


FIG. 2: Shear stress as a function of strain, at constant shear rate, when  $p = 3 > 2$  and  $H = -1/2$ . The colored lines correspond to different shear rates: blue (bottom plot) -  $\dot{\gamma} = 10^{-4}$ , red (top plot) -  $\dot{\gamma} = 10^5$ .

stress is proportional to the square of the strain. The cell orientation measured by the non-diagonal component of the network tensor  $Q_{xy}$  is proportional to the shear rate.

At high shear rate  $\dot{\gamma} \gg H_1$ , larger than the rate of  $T_1$  transitions, the network tensor reaches a steady state with  $Q^{*12} = \frac{A_s}{7^{1/2}}$  and  $Tr \mathbf{Q}^* = (4/7)^{1/6} (\frac{A_s^2 \dot{\gamma}}{k_p})^{1/3}$ . The shear stress can be calculated after performing the base transformation  $\sigma^{xy} = (\frac{4k_p A_s}{7})^{2/3} \dot{\gamma}^{1/3}$ . The variation of the normal stress difference with strain is given in appendix D. At large times it also goes to a constant value  $\sigma^{yy} - \sigma^{xx} \sim \dot{\gamma}^{2/3}$ .

In the presence of active cell divisions (when  $H > -\frac{1}{2}$  and  $\xi_0 \geq 0$ ) a somewhat similar picture arises and is displayed in Fig. 3 and 4. The tissue is elastic at small deformation or at short times, the stress shows an overshoot at intermediate deformations and a plateau at long times. One important result is the existence of a shear homeostatic state at long times where the growth rate vanishes and the observable network tensor has a constant value. At large shear rates, the long time stress plateau does not depend on the shear rate. Additionally, for a hard tissue (when  $p < 2$ ), there is a dynamical transition at the division rate  $\xi_0^* = (1+2H)\frac{4-p^2}{4p}$ , which we already discussed in Ref [13] for the homeostatic pressure. The mechanical properties of the tissue at low strain (or short times) depend on whether the active division rate is smaller or larger than this critical value: for  $\xi_0 < \xi_0^*$  the stress is linear, while for  $\xi_0 > \xi_0^*$  it is close to quadratic (except very close to the critical value  $\xi_0^*$ ). At high shear rates, the steady state stress plateau does not depend on the active division rate  $\xi_0$ . We calculate the high shear rate steady state exponents by power counting as above:  $Q = \det \mathbf{Q} \propto \dot{\gamma}^{-1}$ ,  $Q^{*12} \propto \dot{\gamma}^{-1/2}$ , and  $Tr \mathbf{Q} = const$ . Hence,  $\sigma^{xy} = const$ , and  $\sigma^{yy} - \sigma^{xx} \propto \dot{\gamma}^{1/2}$ . The exact expressions are given in appendix D

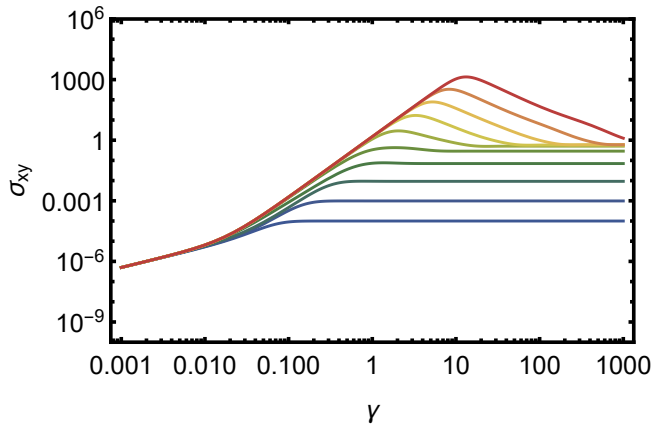


FIG. 3: Shear stress as a function of strain, when  $p = 1.5 < 2$  and  $H = 0$ ,  $\xi_0 = 0.291 < \xi_0^*$ . The colored lines correspond to different shear rates: blue (bottom plot) -  $\dot{\gamma} = 10^{-4}$ , red (top plot) -  $\dot{\gamma} = 10^5$ .

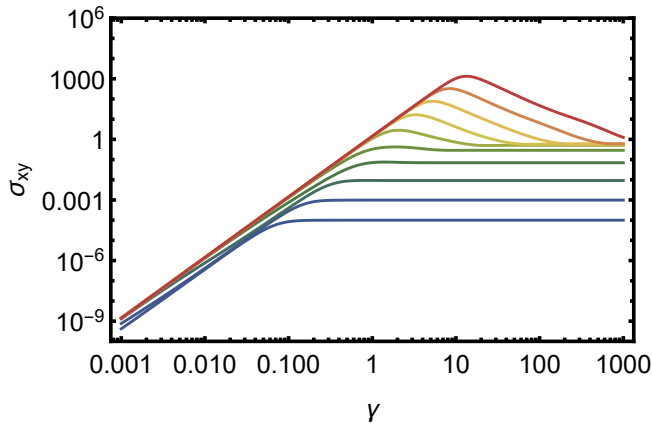


FIG. 4: Shear stress as a function of strain, when  $p = 1.5 < 2$  and  $H = 0$ ,  $\xi_0 = 0.292 > \xi_0^*$ . The colored lines correspond to different shear rates: blue (bottom plot) -  $\dot{\gamma} = 10^{-4}$ , red (top plot) -  $\dot{\gamma} = 10^5$ .

Using a similar approach, we discuss the linear rheology of the tissue at a finite pulsation  $\omega$ . In this experiment, a tissue is sheared in an oscillatory manner so that  $\dot{\gamma} \propto \sin \omega t$ . A soft solid tissue has soft deformation modes and its complex modulus vanishes. The shear aligns the cells in a direction either parallel or perpendicular to the shear. The explicit calculation of the complex shear modulus of a hard solid tissue is given on Fig 5. It is explicitly calculated by linearizing Eq. (8), writing  $\mathbf{Q}^* = \mathbf{Q}^*_0 + \mathbf{Q}^*_1(\omega)e^{-i\omega t}$ , where

$$\mathbf{Q}^*_0 = \begin{pmatrix} q_0 & 0 \\ 0 & q_0 \end{pmatrix}$$

is the free isotropic solution as in Ref. [13], and  $q_0 = \frac{1+2k_p p}{1+4k_p}$  when proliferation is not allowed ( $H = -\frac{1}{2}$ ), or

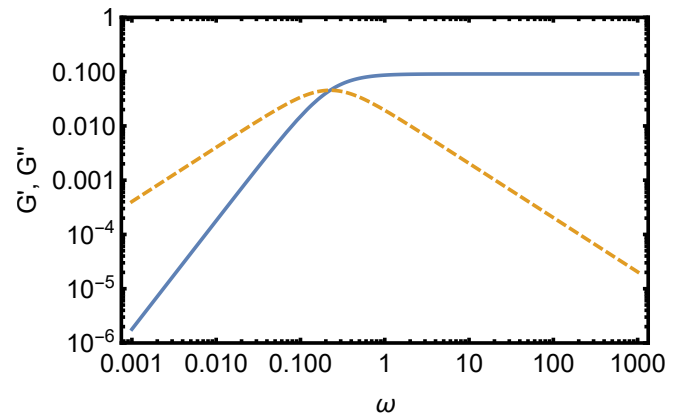


FIG. 5: Linear response of a hard tissue  $p < 2$  under oscillatory forcing, as a function of frequency. This rheology corresponds to that of a viscoelastic Maxwell model. The storage modulus  $G'$  is given by the blue line and the Loss modulus  $G''$  by the dashed yellow line.

$q_0 = \sqrt{\frac{1+k_p p^2}{1+4k_p}}$  when proliferation is allowed ( $H > -\frac{1}{2}$ ). Eq. (8) can then be written as

$$-i\omega \mathbf{Q}^*_1 = -\mathbf{M} \mathbf{Q}^*_1 + \lambda_0 \quad (12)$$

where  $\lambda_0$  is the zeroth order expansion of the term driving the deformation. The components of  $\mathbf{M}$  are explicitly given in appendix C. Within the linear regime, the tissue behaves as a Maxwell fluid with a high frequency shear modulus given by (11) and a viscoelastic relaxation time  $T_r = \frac{1}{4k_p q_0 - 2k_p p}$ . The tissue viscosity is given by the standard Maxwell formula  $\eta = GT_r$ .

## TISSUE ON AN ELASTIC SUBSTRATE

We now consider a tissue forming a confluent monolayer supported by an elastic substrate, with a Poisson ratio  $\nu$ , stretched and relaxed in an oscillatory manner along the  $x$  direction at a pulsation  $\omega$  as studied experimentally in Ref. [15], as explained in the inset of fig. 6. We consider that the tissue strongly coupled to the much stiffer substrate. Therefore, the metric tensor in the tissue is imposed by the elastic deformation of the substrate. Considering the substrate as a thin elastic sheet, we write it as

$$g_{\mu\nu}(t) = \begin{pmatrix} 1 + \alpha \sin^2 \frac{\omega}{2} t & 0 \\ 0 & (1 + \alpha \sin^2 \frac{\omega}{2} t)^{-\nu} \end{pmatrix} \quad (13)$$

where  $\alpha$  is the stretching amplitude.

At the time scales of the experiment in Ref. [15], we consider here that there is no cell division or cell death so that the total number of cells  $N_{cell} = \int \frac{1}{\sqrt{gQ}} \sqrt{g} d^2x$  remains constant. The reason is two fold: first, in what

follows, this allows for an easy decoupling of the tissue's mechanical response relative to the substrate, from the effects of proliferation. Second, this is often the case, as cell division rate is typically tens of minutes to many hours, while the oscillation can be significantly faster [15]. The deformations of the cells are driven by the deformation of the substrate but they do not follow it exactly: over long time scales, cells can change their orientations and their areas from the values imposed by the substrate by detachments from and reattachments to the substrate, which change the network tensor  $\mathbf{Q}$ . Detachments and reattachments therefore play the same role as the topological transitions in the previous section. In a mean field approximation where all cells are identical, the energy given by Eq. (3) can be written as

$$E(t) = N_{cells} \left\{ \left[ \left( 1 + \alpha \sin^2 \frac{\omega}{2} t \right)^{\frac{1-\nu}{2}} \sqrt{Q(t)} - 1 \right]^2 \right. \\ \left. + k_p \left[ \left( 1 + \alpha \sin^2 \frac{\omega}{2} t \right)^2 Q^{xx}(t) \right. \right. \\ \left. \left. + \left( 1 + \alpha \sin^2 \frac{\omega}{2} t \right)^{-\nu} Q^{yy}(t) - p \right]^2 \right\} \quad (14)$$

Since the metric tensor is imposed by the substrate, the network tensor,  $Q^{\mu\nu}$  can relax. The symmetries being the same, we use the relaxation dynamics of (5) in the absence of cell division ( $\xi_0 = 0$ ). In this experiment, the dynamics neighbor exchange ( $T_1$  transitions) but not other topological transitions (proliferation). They are due to attachments and detachments of the cells at a rate  $H_1$  and the dimensionless coefficient  $H$  that controls the area changes during these processes.

If the oscillations are extremely fast,  $\omega \gg H_1 = 1$ , they may be averaged in the vertex energy. (The explicit calculation is given in appendix A). The average energy reads

$$\tilde{E}_{eff} = \frac{2\pi E_{eff}}{N_{Cells}} = \left[ F_{((1-\nu),\alpha)} Q - 2F_{(\frac{1-\nu}{2},\alpha)} \sqrt{Q} + 1 \right] \\ + k_p \left[ F_{(2,\alpha)} (Q^{xx})^2 + F_{(-2\nu,\alpha)} (Q^{yy})^2 + (p)^2 \right. \\ \left. + 2F_{(1-\nu,\alpha)} Q^{xx} Q^{yy} - 2p (F_{(1,\alpha)} Q^{xx} + F_{(-\nu,\alpha)} Q^{yy}) \right]. \quad (15)$$

where  $F_{(\beta,\alpha)} = {}_2F_1\left(\frac{1}{2}, -\beta, 1, -\alpha\right) = \int_{-1}^1 \frac{(1+\alpha x^2)^\beta}{\sqrt{1-x^2}} dx$  is the ordinary hyper-geometric function [17].

After a long time, we assume that the system reaches a steady state and we look for a network tensor  $Q_0^{\mu\nu}$  that minimizes the energy. A complete derivation of the steady state network tensor is given in appendix B.

In Eq. (15), the non-diagonal component of the network tensor  $Q^{xy}$  appears only in the cell area term

through the determinant  $Q$ . It can be chosen as an order parameter for the cell orientation, because if it does not vanish, the network is not oriented along the principal axes of the deformation. In the following, we focus on  $Q^{xy}$  and on the orientation angle of the eigen-direction of the network tensor  $Q^{\mu\nu}$ .

For any oscillation amplitude  $\alpha$ , and Poisson ratio  $\nu$ ,  $Q^{yy} \geq Q^{xx}$ , the component of the network tensor perpendicular to deformation axis is larger than the component parallel to the deformation and we measure the orientation angle with respect to the  $y$  axis. This preferred orientation can be understood from an intuitive argument, that replaces a cell by a thin rod with finite dimensions. For any Poisson ratio  $-1 < \nu < 1$ , the actual change of the rod's length along the  $y$  direction is smaller by a factor of  $\nu$  than along the stretching  $x$  direction. It is therefore in general energetically favorable to align along the perpendicular direction.

Fig. 6 shows the orientation angle of the cells in the case where the shape parameter is  $p = 3$ , corresponding to a "soft" solid behavior. In the absence of any oscillations, the tissue is in an ordered state where all the cells are elongated such that the cell area is  $A = 1$  and  $p = p^0$ . There is a well defined cell orientation which is spontaneously chosen. The figure shows the average angle of the cells with respect to the direction perpendicular to the stretching during the oscillations.

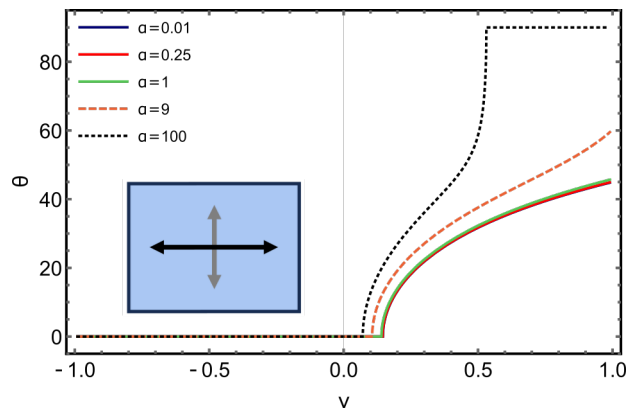


FIG. 6: Average tissue angle of compatible tissues supported on an oscillating elastic medium, as a function of the material's Poisson's ratio, for different oscillation amplitudes. Inset on the lower left - visualization of the forcing mode. Black arrow - stretching axis, grey - substrate response (Poisson's ratio), both force the tissue supported by the substrate.

Several features emerge from the figure. While for  $\nu < 0$ ,  $Q^{12} = 0$  and the cells align perpendicular to the stretching direction, for  $\nu > 0$  there exists a critical value  $\nu^*(\alpha, p)$ , so that for  $\nu > \nu^*$  the cells orient at a finite angle  $\theta$  relative to the direction perpendicular to the stretching. At very large deformations  $\alpha \gg 1$ , the actual average angle during oscillations may reach  $\frac{\pi}{2}$  i.e

- along the stretching direction. This seems contrary to the intuitive argument given above, but for large deformations, the average change of the length of the cell along the stretching direction may be arbitrary large (growing as  $\alpha$ ), while in the perpendicular direction its length vanishes (roughly as  $\alpha^{-2\nu}$ ), so that any finite shape is inevitably extremely elongated.

To understand the existence of finite angle for  $\nu > \nu^*$ , it is sufficient again to consider the case of a finite length rod. In this case, when  $\nu > 0$ , as the  $y$  direction is being stretched, the  $x$  direction contracts, therefore there exists an orientation,  $\psi$ , along which the rod's length does not change. Rather, at this orientation, it rotates. For a thin rod this angle is given by  $\psi = \text{arccot}[\sqrt{\alpha}/\sqrt{2-2F(-\nu,\alpha)}]$  (up to reflections around the principal axes). For a finite cell the range of existence of such an orientation depends on  $p$ . We expect that as  $p \rightarrow \infty$ , the onset of a nontrivial orientation occurs for a value of the Poisson ratio  $\nu^* \rightarrow 0$ , while for  $p < 2$  no such solution can be found. Other properties of the tissue are given in appendix G including the behavior of the tissue just after stopping the oscillations

In the limit  $\alpha \rightarrow 0$ , we expect that the network tensor  $Q^{\mu\nu}$  is close to that of a free standing tissue. However, the existence of a symmetry breaking transition at a finite Poisson ratio  $\nu^*$ , indicates a non perturbative solution. We therefore expand  $\mathbf{Q}(\alpha)$  in the limit  $\alpha \rightarrow 0$  for  $p > 2$ . We call  $\tilde{\mathbf{Q}}$  the value of the network tensor that minimizes the energy (15) when  $\alpha = 0$

$$\tilde{\mathbf{Q}} = \begin{pmatrix} \frac{1}{2}(p - K \cos 2\theta) & \frac{1}{2}K \sin 2\theta \\ \frac{1}{2}K \sin 2\theta & \frac{1}{2}(p + K \cos 2\theta) \end{pmatrix}, \quad (16)$$

where  $K = \sqrt{p^2 - 4}$ . Note that the trace is  $\text{Tr}\tilde{\mathbf{Q}} = p$  and the determinant  $\tilde{Q} = 1$ . The orientation angle  $\theta$  of the eigenvectors of the network tensor with respect to the direction perpendicular to the stretching direction is unknown at this point. In order to find it, we use the general decomposition of a positive definite network tensor,  $Q^{\mu\nu}$  in terms of its trace  $\bar{q}$  determinant  $Q$ , and orientation angle  $\theta$  of its eigenvector

$$Q^{\mu\nu} = \begin{pmatrix} \frac{1}{2}(\bar{q} - K' \cos 2\theta) & \frac{1}{2}K' \sin 2\theta \\ \frac{1}{2}K' \sin 2\theta & \frac{1}{2}(\bar{q} + K' \cos 2\theta) \end{pmatrix}. \quad (17)$$

where  $K' = \sqrt{\bar{q}^2 - 4Q}$ .

We expand  $\bar{q} = p + \alpha\bar{q}_1 + \alpha^2\bar{q}_2$ ,  $Q = 1 + \alpha Q_1 + \alpha^2 Q_2$ , and the network tensor, which minimizes the energy (15) up to second order in the amplitude  $\alpha$ . The minimization of the energy gives an angle  $\theta$  independent of  $\alpha$ . There is therefore a non-analytical symmetry breaking solution driven by the perturbation due to the stretching.

$$\theta = \begin{cases} \frac{\pi}{2} \pm \frac{1}{2} \arccos\left(-\frac{p}{\sqrt{p^2-4}} \frac{1-\nu}{1+\nu}\right), & \nu \geq \nu^* \\ 0, & \nu < \nu^* \end{cases} \quad (18)$$

where the sign corresponds to the remaining reflection symmetry, and  $\nu^* = \frac{p-\sqrt{p^2-4}}{p+\sqrt{p^2-4}}$ . For any  $\nu > \nu^*$ ,  $\theta \neq 0$  and  $\theta(\nu = 1) = \pi/4$ .

When  $p < 2$ , in the limit of small amplitude  $\alpha \rightarrow 0$ , the network tensor is isotropic

$$\tilde{Q}^{\mu\nu} = \begin{pmatrix} \frac{1+2k_p p}{1+4k_p} & 0 \\ 0 & \frac{1+2pk_p}{1+4k_p} \end{pmatrix}. \quad (19)$$

For a tissue on a stretched substrate, the rheology at finite pulsation  $\omega$  can be discussed as in the previous section. We use the same procedure as for the shear geometry and perform the change of reference frame to the real coordinates given by (7). The relaxation dynamics of the network tensor is given by (5) in the absence of cell divisions ( $\xi_0 = 0$ ). Note however that the field  $\eta = \frac{\delta E}{\delta \mathbf{Q}}$  conjugate to the network tensor must be calculated at constant number of cells. This is done by introducing the energy per cell  $e$  such that  $E = N_{\text{cell}} \mathcal{E}$ . The conjugate field is then calculated as  $\eta = \rho \frac{\partial \mathcal{E}}{\partial \mathbf{Q}}$ . The relaxation dynamics of the observable network tensor is given by

$$\begin{aligned} \partial_t \mathbf{Q}^* &= -\sqrt{Q^*} \left( \sqrt{Q^*} - 1 \right) (1 + 2H) \mathbf{Q}^* \quad (20) \\ &\quad - 2k_p \mathbf{Q}^* (\text{Tr} \mathbf{Q}^* - p) (\mathbf{Q}^* + H \text{Tr} \mathbf{Q}^*) \\ &\quad + \lambda, \end{aligned}$$

where the driving term is

$$\lambda = \begin{pmatrix} 2f(\omega, t, \alpha) Q^{*11} & (1-\nu)f(\omega, t, \alpha) Q^{*12} \\ (1-\nu)f(\omega, t, \alpha) Q^{*12} & -2\nu f(\omega, t, \alpha) Q^{*22} \end{pmatrix} \quad (21)$$

with a driving function  $f(\omega, t, \alpha) = \frac{\alpha\omega}{4} \frac{\sin \omega t}{1 + \alpha \sin^2 \frac{\omega}{2} t}$

The geometry induces a highly non-linear driving term and we only study here the properties of the tissue at linear order in the amplitude of the oscillation. The linear response is given by (12). Here the small parameter is the amplitude  $\alpha$ , and we use complex notations replacing  $\sin(\omega t)$  with the complex exponent  $e^{-i\omega t}$ .

For a tissue on a substrate, the stress response of the tissue is less important experimentally as the measured stress would correspond to the sum of the substrate stress and the tissue stress  $\sigma_1$ , and by assumption, the substrate is much stiffer than the tissue. We give the calculated value of the tissue stress in appendix F. The results of the hard tissue are similar to those in the previous section and the tissue behaves as a Maxwell visco-elastic fluid with the modulus and relaxation time obtained in the previous section.

In order to calculate the finite frequency response of a soft tissue, we expanded the network tensor  $\mathbf{Q}$  around the ground state with a definite, yet still unknown:  $\mathbf{Q}^* = \tilde{\mathbf{Q}}(\theta) + \mathbf{Q}^*_1$ . We then solved for  $\mathbf{Q}^*_1$  and calcu-

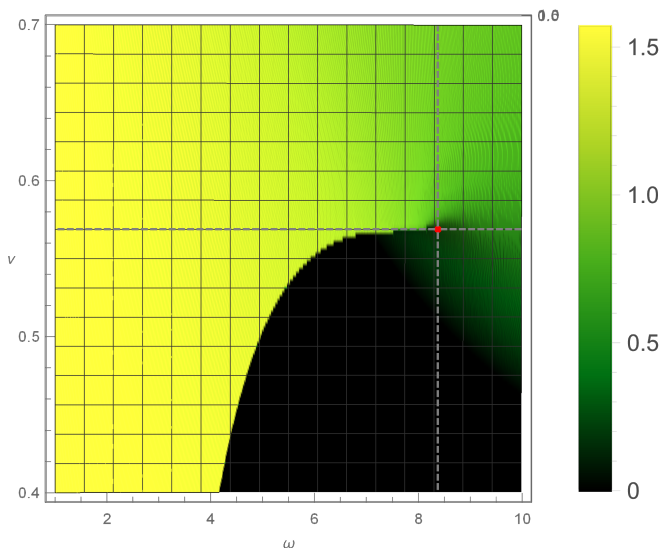


FIG. 7: Tricritical behavior of the cells average orientation  $\theta(\omega, \nu)$ , as a function of frequency,  $\omega$ , and Poisson's ratio,  $\nu$ . The colors corresponds to the values of the angle  $\theta$ : dark green -  $\theta = 0$ , bright yellow =  $\theta = \pi/2$ . Here  $k_p = 1$ ,  $p = 3$   $H = 0$ . Red dot marks the tricritical point ( $\omega_c \sim 8.5$   $\nu_c \sim 0.53$ ) Above  $\omega_c$  the transition is continuous, as indicated by the smooth color gradient. Below the critical value, the transition is discontinuous.  $\theta = 0$  corresponds to cell oriented perpendicular to the main stretching direction,  $\theta = \pi/2$  corresponds to a parallel orientation to the stretching.

lated the angle that minimizes the energy  $E(\tilde{\mathbf{Q}}(\theta) + \mathbf{Q}^*_1)$  expanded to second order in the amplitude  $\alpha$ . We anticipated here that the periodic forcing leads at very long times to a steady state static solution, breaking the rotational symmetry.

The resulting phase space  $\theta(\omega, \nu)$  is quite complicated, and exhibits a tricritical point. We show in Fig. 7 the detailed phase diagram around the tricritical point  $\omega_c \sim 8.5$ , and  $\nu_c \sim 0.58$ . More details on the phase space and the tricritical point are given in appendix H.

## Discussion

This paper discusses the macroscopic mechanical properties of an epithelial two dimensional tissue starting from the cellular vertex model introduced in reference [13]. As emphasized in this work, the rheology of the tissue strongly depends on the existence of internal stresses in the tissue (hard solid for a shape factor  $p < 2$ ) or on soft modes (soft solids for a shape factor  $p > 2$ ). We study explicitly two geometries, a sheared tissue and a tissue on a stretched elastic substrate.

The main result of our work is an explicit analytical calculation of the rheological properties of a tissue, using

a coarse-grained model that is rigorously derived from a detailed, discrete, vertex model. An important general result is that the tissues can be considered as thixotropic fluids. After the application of a constant shear rate the tissues are elastic at short time with a finite shear modulus for hard tissues and a vanishing shear modulus for soft tissues. As the strain is increased, the stress goes through a maximum and then decreases to a plateau that depends only of the applied shear rate. At small shear rates the tissue is liquid with a finite viscosity. At large shear rates, the tissue is shear thinning and the stress increases as a power law of the shear rate. As in previous numerical studies [18, 19], we never find a finite yield stress even in the absence of cell proliferation. The stress always relaxes because of the cell rearrangements due to the  $T_1$  topological processes (or due to proliferation if present). A shear thinning behavior has already been observed in numerical particle simulations, or predicted in simplified models for tissues in Ref. [9, 19].

An important result for proliferating tissues is the existence of a shear homeostatic state which is a steady state of the tissue under shear where cell division exactly compensates cell death. In this steady state the tissue has plastic behavior where at long times the stress reaches a plateau independent of shear rate and of the active division rate.

We also discussed the linear rheological behavior at finite frequency of hard tissues. They behave as Maxwell fluids with a finite relaxation time due to the topological transformations in the tissue in line with previous work on cell division [5]. Because of the presence of soft modes, the linear complex modulus of soft tissues vanishes.

This general picture of two-dimensional tissue rheology seems to be robust as attested by the existing numerical simulations of tissues. Our results also share some similarities with the rheology of foams [20–22]. Still some details of the predictions such as the shear thinning exponent  $1/3$  might depend on the precise assumptions made for the transport coefficient  $\Gamma^{\mu\nu\alpha\beta}$  in Eq. (5). We chose the simplest transport coefficient compatible with the symmetries and that depends only on the network tensor which is the tensor that we use to characterize the topological transitions in the tissue. Contributions of the metric tensor and more general non-linear terms in order to go beyond the geometric non-linearities could be introduced and modify the shear thinning exponent. We also have considered that the metric tensor measuring elastic effects relaxes instantaneously, which is certainly not true at high frequencies. The elastic relaxation could be taken into account by the introduction of a short time viscosity.

The second geometry that we considered is that of experiments measuring cell orientation under periodic stretch of an elastic substrate. Only elongated cells orient under stretch, corresponding to soft tissues. If the stretching is performed at high frequencies, our results

at small amplitudes are very similar to those obtained from a macroscopic elastic description of the tissue as a uniaxial material [15, 23, 24]. We provide here extensions of these results to non-linear stretching amplitudes and to finite frequencies.

Finally, we only considered homogeneous uniform tissues. Adding seams or non-uniform regions where the tissue might be stiffer (simulating scars), or just has a different topology (such as a hole) can shed important light on the way tissues heal and help better understand how scars affect the mechanical response of an organ.

---

\* doron.grossman@ladhyx.polytechnique.fr

- [1] V. Mirabet, P. Das, A. Boudaoud, and O. Hamant, The role of mechanical forces in plant morphogenesis, *Annual review of plant biology* **62**, 365 (2011).
- [2] A. Goriely, *The mathematics and mechanics of biological growth*, Vol. 45 (Springer, 2017).
- [3] C. Blanch-Mercader, R. Vincent, E. Bazellières, X. Serra-Picamal, X. Trepas, and J. Casademunt, Effective viscosity and dynamics of spreading epithelia: a solvable model, *Soft Matter* **13**, 1235 (2017).
- [4] D. W. Thompson and D. W. Thompson, *On growth and form*, Vol. 2 (Cambridge university press Cambridge, 1942).
- [5] J. Ranft, M. Basan, J. Elgeti, J.-F. Joanny, J. Prost, and F. Jülicher, Fluidization of tissues by cell division and apoptosis, *Proceedings of the National Academy of Sciences* **107**, 20863 (2010).
- [6] E. Hannezo, J. Prost, and J.-F. Joanny, Theory of epithelial sheet morphology in three dimensions, *Proceedings of the National Academy of Sciences* **111**, 27 (2014).
- [7] R. Farhadifar, J.-C. Röper, B. Aigouy, S. Eaton, and F. Jülicher, The influence of cell mechanics, cell-cell interactions, and proliferation on epithelial packing, *Current Biology* **17**, 2095 (2007).
- [8] D. B. Staple, R. Farhadifar, J.-C. Röper, B. Aigouy, S. Eaton, and F. Jülicher, Mechanics and remodelling of cell packings in epithelia, *The European Physical Journal E* **33**, 117 (2010).
- [9] S. Ishihara, P. Marcq, and K. Sugimura, From cells to tissue: A continuum model of epithelial mechanics, *Physical Review E* **96**, 022418 (2017).
- [10] S. Tong, R. Sknepnek, and A. Košmrlj, Linear viscoelastic response of the vertex model with internal and external dissipation: Normal modes analysis, *Physical Review Research* **5**, 013143 (2023).
- [11] R. Etournay, M. Popović, M. Merkel, A. Nandi, C. Blasse, B. Aigouy, H. Brandl, G. Myers, G. Salbreux, F. Jülicher, *et al.*, Interplay of cell dynamics and epithelial tension during morphogenesis of the drosophila pupal wing, *Elife* **4**, e07090 (2015).
- [12] B. Guirao, S. U. Rigaud, F. Bosveld, A. Bailles, J. Lopez-Gay, S. Ishihara, K. Sugimura, F. Graner, and Y. Bellaïche, Unified quantitative characterization of epithelial tissue development, *Elife* **4**, e08519 (2015).
- [13] D. Grossman and J.-F. Joanny, Instabilities and geometry of growing tissues, *Phys. Rev. Lett.* **129**, 048102 (2022).
- [14] M. Moshe, M. J. Bowick, and M. C. Marchetti, Geometric frustration and solid-solid transitions in model 2d tissue, *Physical review letters* **120**, 268105 (2018).
- [15] L. Géréme, E. Ilker, M. Bernheim-Dennery, C. Cavaniol, J.-L. Viovy, D. M. Vignjevic, J.-F. Joanny, and S. Descroix, Evolution of a confluent gut epithelium under on-chip cyclic stretching, *Physical Review Research* **4**, 023032 (2022).
- [16] G. Lucci, C. Givero, and L. Preziosi, Cell orientation under stretch: Stability of a linear viscoelastic model, *Mathematical Biosciences* **337**, 108630 (2021).
- [17] W. N. Bailey, Generalized hypergeometric series, (No Title) (1935).
- [18] D. Matoz-Fernandez, K. Martens, R. Sknepnek, J. Barrat, and S. Henkes, Cell division and death inhibit glassy behaviour of confluent tissues, *Soft matter* **13**, 3205 (2017).
- [19] M. Basan, J. Prost, J.-F. Joanny, and J. Elgeti, Dissipative particle dynamics simulations for biological tissues: rheology and competition, *Physical biology* **8**, 026014 (2011).
- [20] S. A. Khan, C. A. Schnepfer, and R. C. Armstrong, Foam rheology: Iii. measurement of shear flow properties, *Journal of Rheology* **32**, 69 (1988).
- [21] A. M. Kraynik, Foam flows, *Annual Review of Fluid Mechanics* **20**, 325 (1988).
- [22] J. Sibree, The viscosity of froth, *Transactions of the Faraday Society* **30**, 325 (1934).
- [23] A. Livne, E. Bouchbinder, and B. Geiger, Cell reorientation under cyclic stretching, *Nature communications* **5**, 3938 (2014).
- [24] A. Moriel, A. Livne, and E. Bouchbinder, Cellular orientational fluctuations, rotational diffusion and nematic order under periodic driving, *Soft matter* **18**, 7091 (2022).